Materials International
Open-Access Journal (ISSN: 2668-5728)

Article
Volume 8, Issue 2, 2026, 11
https://doi.org/10.33263/Materials82.011

Synthesis Spectral Characterization of Al_2O_3-ZnO Doped Nanocatalyst for Electrochemical Behavior of 4-Nitrophenol

Shwetha Heddur Krishnamurthy [1], Shreekanta Sasigolli Annappa [1,], Sachin Haluvally Puttaswamygowda [2], Malathesh P [3]

[1] Department of Studies and Research In Chemistry, Sahyadri Science College, Kuvempu University, Shimoga, Karnataka,577203, India
[2]Department of Chemistry, Jawaharlal Nehru New College of Engineering(JNNCE), Shivamogga-577204, Karnataka, India[3]Department of Chemistry, BGS Institute of Technology(BGSIT), Adichunchanagiri University, BG Nagara, Nagamangala, Karnataka, India 571448
* Correspondence: shreekanta.camistryi@gmail.com;

Received: 17.07.2025; Accepted: 29.10.2025; Published: 10.06.2026

Abstract: In this study, Al_2O_3-ZnO nanocomposite (NC) was synthesized via a simple combustion method. The prepared NC was characterized using XRD, FTIR, UV-Visible, TGA, and SEM. XRD data match the JCPDS standards 5-661 and 78-429, corresponding to Al_2O_3, ZnO, and NC, respectively. The formation of the nanocomposite and the functional groups present in the sample can be confirmed by FTIR and UV-Vis spectroscopic studies. The FT-IR spectrum shows the presence of metal-oxygen bonding in the Al2O3-ZnO NC, the high thermal stability of the sample, as confirmed by TGA, and the surface morphology, as confirmed by SEM, indicating the uniform distribution of the nanocomposite. The analytical profile of the composite modified electrode (Al_2O_3-ZnO)/(GCE) demonstrated that it is an effective nanoparticle composite electrode for the electrochemical detection of 4-Nitrophenol (4NP), with a wide linear detection range of 10 to 70 µmol/L. Also, a low detection limit (LOD) of 3.666 µM/L and excellent sensitivity of 0.0153 $\mu M^{-1}$and R^2 is 0.9951. To calculate the sensitivity of an electrochemical phenol detection, use the slope of the calibration curve and the LOD for the electrochemical detection of phenol. The most common formula is LOD = 3σ/S, where σ is the standard deviation of the blank signal, and S is the slope of the calibration curve. It is therefore the modified electrode that has become a good electrode material, with notable stability and no leaching.

Keywords: ZnO; Al_2O_3; Al_2O_3-ZnO; spectral characterization; cyclic voltammetry; 4-NP.

1. Introduction

The monitoring of aromatic nitro-compounds, including nitrobenzene and nitrotoluenes, in aquatic systems and industrial discharges is critical for controlling regeneration due to their occurrence from a wide range of activities [1]. These substances have toxic effects on humans' biological systems, animals, and plants, and impart undesirable taste and odor to drinking water, even at very low concentrations [2]. For regulatory purposes, frameworks globally now encompass numerous nitrocompounds, including 4-nitrophenol (4-NP), specifically by the U.S. Environmental Protection Agency (EPA) because of its toxic

nature and long-term persistence in the environment [3]. Short-term exposure NP through inhalation or ingestion in humans may result in headaches, drowsiness, nausea, and cyanosis [1]. Furthermore, 4-NP has been shown to exhibit suspected carcinogenic, teratogenic, and mutagenic activity in model organisms [4]; therefore, its application should be strictly regulated and closely monitored. Nevertheless, 4-NP is still widely used as an intermediate in the manufacture of pharmaceuticals, dyes, pesticides, and insecticides, such as fenitrothion and parathion, which can undergo reversible hydrolysis to release 4-NP [5, 6]. Therefore, during its production and use in industry and agrochemicals, 4-NP will unavoidably be released into the environment, causing pollution. Therefore, the development of an easy-to-use and trustworthy method for detecting traces of 4-NP in the environment is crucial and urgent. Spectrophotometry [7], fluorescence [8], gas chromatography (GC) [9], capillary electrophoresis, and high-performance liquid chromatography (HPLC) [10]. Traditional spectrophotometric and colorimetric methods can be easily compromised by interfering compounds. HPLC and capillary electrophoresis are excellent alternative methods, but they require high purchase costs for columns and the use of organic solvents [11]. Generates significant west, creating a strong demand for now analytical techniques that rely on inexpensive and readily available equipment. Such methods should be low-cost, simple to implement, time-efficient, and capable of real-time detection of 4-NP. In addition, the electrochemical reducibility of nitro groups on aromatic or heterocyclic rings, well documented in the literature enables the determination of numerous genotoxic and ecotoxic nitrocompounds using modern voltametric techniques with modified electrode recently Mhammedi *et al*. [12] reported the use of a hydroxyl apatite-modified electrode to study the electrochemical behavior of 4-NP, achieving a low detection limit of 8nM, furthermore several other modified electrodes, particularly those based on carbonnanotubes[13-15], have also been developed for this purpose. nano-gold[16], silver particles[17], and ionic liquid[18] have also been reported to detect 4-NP with satisfactory results. However, there is still a strong need for simpler preparation methods to develop new electrochemical sensors based on advanced materials with excellent electrochemical properties. Al_2O_3 and ZnO nanoparticles produced by combustion methods have attracted significant interest across a variety of fields due to their extensive research applicability, including electronics, drug delivery systems, energy-efficient systems, chemical engineering, and medicine [15–17]. Studies have reported the preparation of γ-Al2O3 QDs via a cost-effective hydrothermal process and their characterization in detail using various instruments. The γ-Al_2O_3QDs were used as the sensor material to form a layer on GCE. Urea (SBA-U) and aloe vera (SBA-A) extracts are used as a fuel/reducing agent for the synthesis of SrO/BaO/Al2O3 (SBA) NCs by the solution combustion method. Similarly, another green synthesis study uses Rhus punjabensis extract to prepare Fe2O4 nanoparticles. Furthermore, these particles exhibited both anticancer and antimicrobial properties [19]. The rapidly developing nanotechnology exposes humans to nanoparticles in several ways (e.g., inhalation, ingestion, and skin contact). Furthermore, nanoparticles can penetrate other important organs and pathways, including cells. Al_2O_3-ZnO NCs were created and used for photocatalytic and sensing applications, and they have shown superior performance compared to the individual oxides. In this study, we synthesized pure Al_2O_3-ZnO NC NP and Al_2O_3-ZnO NC using Amul milk powder as our fuel source. Production can be achieved in three main ways: physical and biological. Because noble metals such as gold, silver, and Platinum nanoparticles are widely used in human contact areas, various possible biomedical applications have been evaluated [20, 21]. Researchers successfully tested a variety of metals and metal oxide nanoparticles prepared

via biological pathways; however, few bimetallic nanocomposite particles have been reported using a combustion method. Here, we attempt to synthesize Al_2O_3, ZnO, and Al_2O_3-ZnO NC nanoparticles via a combustion method using a fuel. Mediated combustion methods are identified, and a prepared sample is characterized for its structure by X-ray diffraction (XRD), morphology by scanning electron microscopy (SEM), and bonding by Fourier transform infrared (FT-IR) spectroscopy. Cyclic voltammetry is a potentiodynamic electrochemical technique known to be simple, inexpensive, rapid, reliable, and trustworthy for detecting molecules. This method is used to examine the electrochemical properties of an analyte in solution or of a compound adsorbed on the electrode surface. Over the years, the detection of biomolecules, pollutants, and toxic compounds has become increasingly significant to the scientific community. The aim of this work is to fabricate a novel and stable electrochemical sensor for ultra-sensitive determination of 4-NP.The working electrode was modified with Al_2O_3-ZnO. Compared with the bare electrode, the electrode modified with metal oxides (Al_2O_3-ZnO) exhibited a significantly enhanced response and can be effectively used as an analytical signal for the determination of 4-NP. The propylene glycol method was successfully applied to the detection of trace levels of 4-NP in real water samples, yielding satisfactory results. All experiments were conducted at room temperature, and electrochemical measurements were performed under the same conditions.

2. Materials and Methods

The required analytical-grade chemicals were used from Merck (Mumbai, India). Aluminum sulfate, Zinc sulfate, PVA, ammonium persulfate (APS), Conc.HCl, Conc.HNO_3, sodium chloride (NaCl), and double-distilled water were purchased from Sigma Aldrich. DMF was purchased from Sigma Aldrich. PVA is used in nanomaterial synthesis because it acts as a stabilizing agent, a template for creating specific nanostructures, and it creates functional nanomaterials for applications like biomedical devices, sensors, and fuel cells

2.1. Instruments and apparatus.

Cyclic voltammetry measurements were performed using a CH Instruments electrochemical analyzer connected to a PC. Electrochemical measurements were performed in an electrochemical cell containing a platinum wire of 5 cm^{-1} as auxiliary electrode, a silver/silver chloride electrode (Ag/AgCl saturated with KCl) as reference, and a glassy carbon electrode with 0.44 cm (Pine Instruments, U.S.) as working electrode. All experiments were done at room temperature. All the electrochemical measurements were carried out on a CHI608D electrochemical workstation (Shanghai Chenhua Instrument Co., Ltd., China) with a conventional three-electrode system (GCE, Platinum Wire Electrode, and Ag/AgCl electrode). A glassy carbon electrode (3 mm in diameter) loaded with different materials was used as the working electrode. UV-Vis absorption spectra were measured at room temperature on a Shimadzu UV-550 spectrophotometer using a 1 cm pathlength cuvette for solution studies. Infrared (IR) spectra were recorded using the PerkinElmer Spectrum 100 FT-IR Spectrometer. X-ray diffraction measurements (XRD) (Cu Ka radiation) were performed using a Bruker Advanced D8 diffractometer. Thermogravimetric analyses (TGA) were performed on a Mettler Toledo instrument with a heating rate of 20°C/min and a nitrogen flow rate of 50 mL/minute. The GCE surface was polished with 0.3 and 0.05 μM alumina slurries, then sequentially

ultrasonicated in water and ethanol. Then the bare GCE was dried under pure N_2. Finally, these materials were dropped on the surface of bare GCE and dried at room temperature.

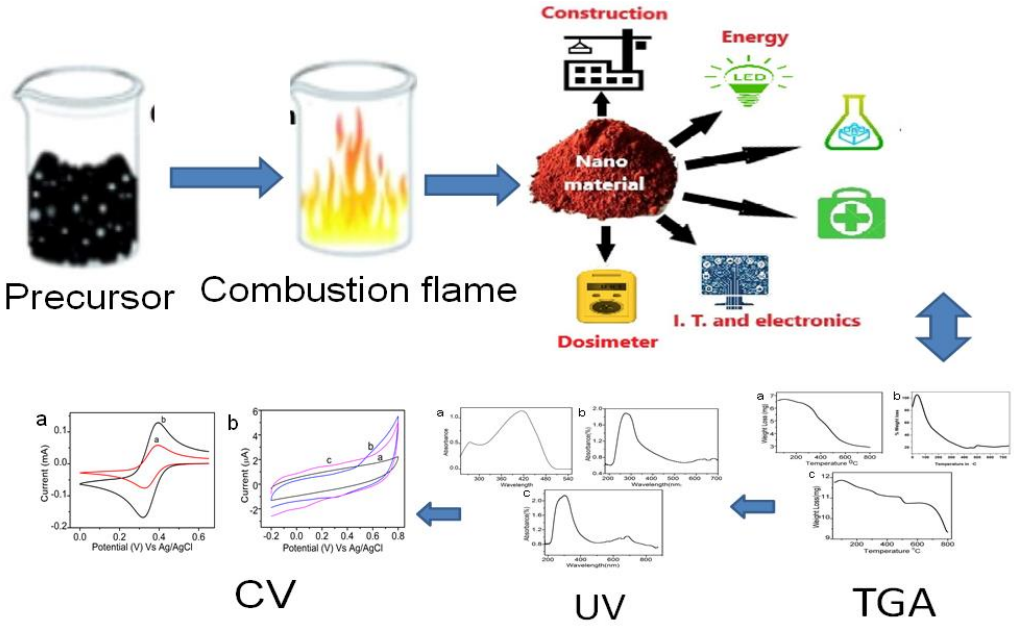

Scheme 1. Schematic diagram summarizing synthesis and characterization steps.

2.2. Synthesis of zinc oxide and aluminum oxide nanomaterials.

Zinc sulfate mixed with PVA in the weight ratio 1:5 and ground well in a pestle and mortar. Here, PVA was used in nanomaterial preparation primarily as a stabilizer and reducing agent, and it also acts as a reducing agent, converting metal salts into nanoparticles *in situ*, and as a host matrix for creating polymer nanocomposites. The resultant solid is transferred into a china dish and heated in air until the carbon dioxide is completely evolved. Then it is transferred into a silica crucible and ignited at 800°C. It was observed that PVA initially melted, then frothed, and finally ignited at 800°C in a muffler furnace, leaving zinc oxide as the residue. Upon cooling to room temperature, a white zinc oxide residue was obtained (Figure 1b). This reaction, which occurs with the evolution of many gases and ignites spontaneously, is called self-propagating combustion [22]. Similarly, aluminum oxide was synthesized by weighing aluminum sulfate and PVA in a 1:5 ratio and grinding them thoroughly in a mortar and pestle, as shown in Scheme 1. The resultant solid is transferred to a china dish and heated in air until all carbon dioxide is evolved. Then it is transferred to a silica crucible and heated to 800°C. It was observed that PVA initially melted, then frothed, and finally ignited at 800°C in a muffler furnace, leaving aluminum oxide as the residue (Figure 1 b).

2.3. Synthesis of zinc aluminate.

Zinc aluminate was synthesized by weighing Zinc oxide, aluminum oxide, and PVA in the ratio 1:1:5 and grinding them well in a pestle and mortar (Figure 1). The resultant solid is transferred to a china dish and heated in the air. Until the carbon dioxide was completely evolved. The resultant ashes were well-ground, transferred to a silica crucible, and ignited at 800°C. It was observed that PVA initially melted, then frothed, and finally ignited at 800°C in a muffler furnace, leaving zinc aluminate as the residue. The results are shown in Scheme 1.

2.4. Characterization technique.

The prepared nanostructure of Al_2O_3, ZnO, and Al_2O_3-ZnO was analyzed by recording the XRD data of the sample using Rigaku-Smart lab X-ray diffractometer with CuKa (λ= 1.54 Å) radiation. Fourier-transform infrared (FT-IR) spectrum was obtained with a Bruker Alpha-p spectrometer from a KBr pellet method. Morphology was examined by scanning electron microscopy (SEM) on JOEL NeoScope JCM-6000PLUS, along with energy dispersive analysis of X-ray spectroscopy (EDAX). The UV-visible absorption spectra of the prepared NPs were measured using an Agilent Technologies Cary 60 UV-Vis spectrophotometer. A CH-instrument, CHI608D, made in the USA, has been used for electrochemical explorations.

3. Results and Discussion

3.1. UV-vis study.

The surface plasma on the 410 nm resonance peak in Figure 1a indicates the presence of Al_2O_3 nanoparticles, while the peak at 320 nm indicates the presence of ZnO nanoparticles, as shown in Figure 1b. Furthermore, the UV-absorbing peak is observed at 380 nm, with a shoulder at 520 nm in Figure 1c. In these spectra of Al_2O_3-ZnO nanoparticles, the maximum in the UV region indicates the characteristic absorption edge of the metal oxide nanoparticles. The red shift observed in all spectra indicates the formation of nanosized particles containing metal oxides. These spectra are compared to the UV spectra of the basic connection shown in Figure 1. The absorbing range for these nanoparticles, compared to the metal oxides specified in the reported work, is roughly the same [23-25].

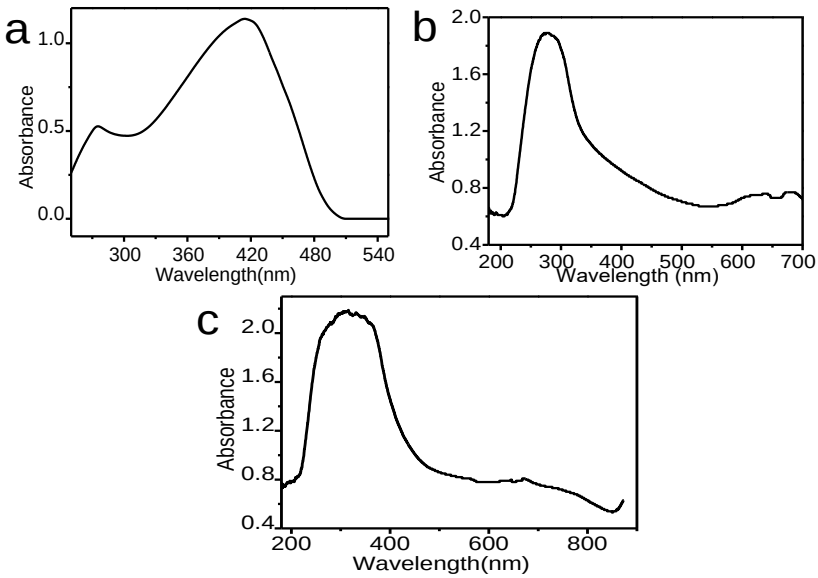

Figure 1. UV spectra of **(a)** Al_2O_3 sample; **(b)** ZnO sample; **(c)** Al_2O_3-ZnO nanoparticles.

The direct energy band gap is 20 eV, calculated using the Kubelka-Munk function by plotting the tangents versus photon energy (eV).

$$F((R\infty) = (1 - R\infty)2/2R\infty \quad (1)$$

The band gap of the synthesized AlO, ZnO, and AlO-ZnO NPs was found to be 3.32, 3.62, and 3.68 eV, respectively, as shown in Figure 2.

Table 1. Band gap study of the compound AlO, ZnO, and AlO-ZnO.

Compounds	Band gap (eV)
AlO	3.32
ZnO	3.62
AlO-ZnO	3.68

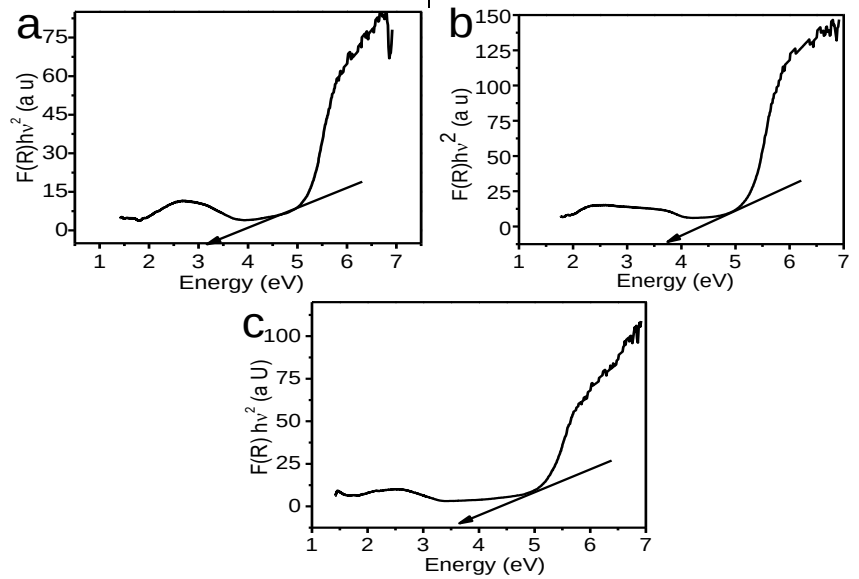

Figure 2. UV DRS Spectra and band gap energy of **(a)** AlO nanoparticles; **(b)** ZnO; **(c)** AlO-ZnO nanoparticles.

3.2. Infrared study.

The bonding characteristics of the metal oxide samples were investigated using FTIR spectroscopy. The recorded spectra, shown in the figures, reveal that all metal oxide samples exhibit a broad absorption band at 3300-3500 cm-1, attributed to adsorbed water molecules. Peaks observed around 1500-1550 cm^{-1} correspond to CH stretching vibrations, while bands in the 1450-1500 cm^{-1} region arise from overtone vibrations of the same bonds. In addition, metal oxides typically display absorption bands below 1000 cm^{-1}, which are associated with the intratomic metal-oxygen vibration modes [26]. The peaks correspond to the vibration modes of the spinal connections (Al2O3 and ZnO) and are attributed to their characteristics.

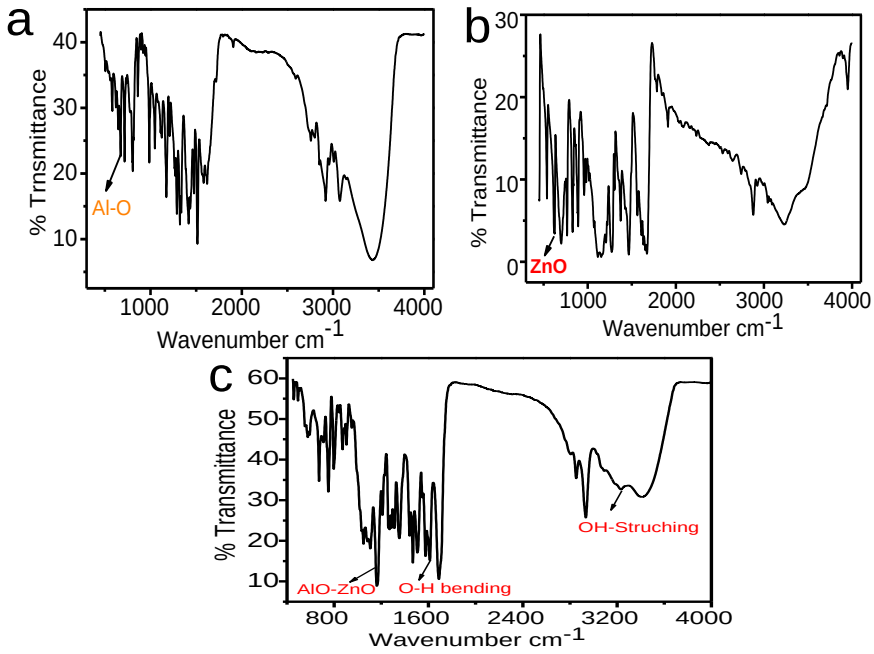

Figure 3. FTIR spectra of **(a)** Undoped Al_2O_3; **(b)** ZnO; **(c)** Al_2O3- ZnO.

3.3. Thermal analysis.

The TGA experiment was performed using 10 mg of the synthesized sample at a heating rate of 5°C/min in static air, as shown in Figure S1. The TGA curve shows three stages of weight loss at different temperatures. In the first step, the weight loss at 100°C is due to the loss of lattice water molecules. The second step of weight loss has occurred at 223°C, corresponding to an exothermic reaction at 250.56°C. The first decomposition starts at 100°C due to the loss of a water molecule. The second decomposition occurred at 100-300°C because of decomposition processes of the organic matter, more pronounced for Al_2–O, and Zn–O. The final decomposition occurred at 700°C. This is due to the conversion of reactant to product [27-30].

3.4. X-ray diffraction.

The X-ray Diffraction pattern of Al_2O_3, ZnO, and Al_2O_3- ZnO was obtained using an XRD powder Diffractometer Shimadzu model: XRD 6000 with CuKα radiation in the range of 20-70° (λ=0.154nm). On the other hand, Figures 4a, b, and c illustrate the XRD patterns of undoped and doped nanosized particles resulting from solution combustion. The hexagonal wurtzite phase of ZnO exhibits the characteristic XRD patterns for Al-doped ZnO composites, and the diffraction data are consistent with the pattern, which matches the 16th standard JCPDS card no. 089-051. The peaks at 22, 28, 34°, 44°, 66°, 74° were assigned to [100], [002], [101], [102], [110], [103], [201], [112], [200] and [004] respectively for Zn-O respectively [31, 32]. The XRD pattern of pure Al-O shows the diffraction peak at the 2θ degrees of 24, 26, 30, 33, 42, 48, 52, 55, 62 and 75 which are corresponds to the crystal plane of Hexagonal [004], [104], [105], [106], [110], [112], [118], [023] and [204] respectively for AlO which is confirmed by the JCPCDS card no. 65–2023, which is shown in Figure 4b [33]. The diffraction peak at 2 θ degrees of 22, 32, 33, 34, 36, 40, 47, 47, 53, 57, 63, 66, 70, 76 and 78 which are corresponds to the crystal plane of [006], [100], [104], [106], [101], [108], [110], [102], [116], [110], [103], [201], [200], [202] and [004] respectively for AlO/ZnO. The average crystallite sizes were determined to be 18 (2θ=36, 42, 66) and found to be 12, 23, 18, 14, and 08 nm. Scherrer's Debye formula was used to determine the crystallite's size (equation 2).

$$D = K\lambda/(\beta cos\theta) \qquad (2)$$

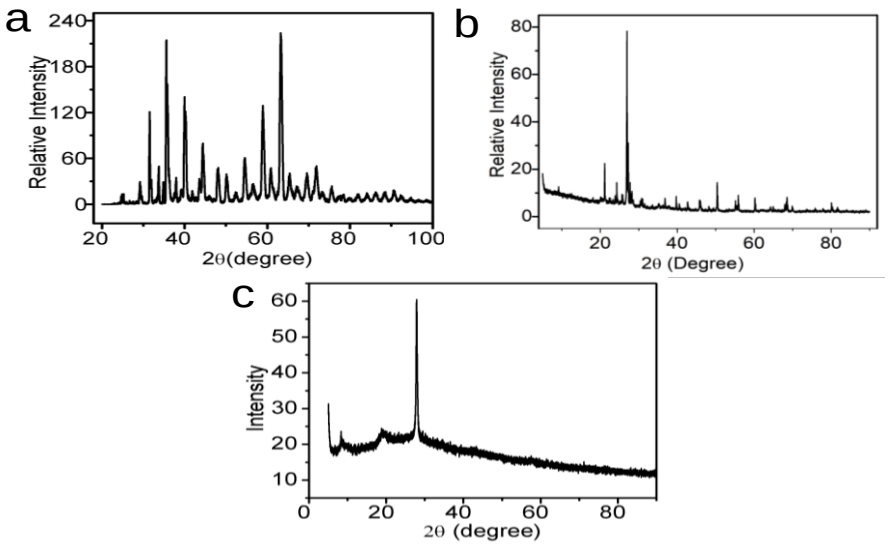

Figure 4. XRD pattern of **(a)** Al_2O_3; **(b)** ZnO; **(c)** Al_2O_3-ZnO samples.

In equation (2), β is the line width at half-maximum height; D is the crystal size; the X-ray wavelength is 0.16506 nm for CuKα, and K is typically taken to be 0.96. The formula produces Al_2O_3 crystallites with diameters of 6.34 nm and thicknesses of 6.4 nm due to ZnO doping. This demonstrates that the ZnO ions are evenly distributed throughout the Al_2O_3 matrix. 2θ°=10-85°, Pure Al_2O_3-crystal planes exhibit similar diffraction peaks to Al_2O_3- ZnO crystal planes. The average size of the crystal of Al_2O_3 and ZnO, Al-doped ZnO, and nanosized particles was determined, and ZnO had no discernible effect on the average crystal size.

3.5. SEM- studies.

The SEM images are shown in Figure 5 for (a) Al_2O_3, (b) ZnO, and (c) Al_2O_3-ZnO composite nanoparticles. Figure 5a illustrates that Al_2O_3 and ZnO nanoparticles are assembled and appear as silt and as micro/nanoparticles. Once the Al_2O_3 nanoparticle is doped with ZnO, a spherulitic structure has been observed in SEM images of Al_2O_3-ZnO nanoparticles, indicating a uniform spherical shape, with the nanoparticles arranged in clusters and a large degree of surface homogeneity. Figure 5a-c represents the SEM images of capped and uncapped nanoparticles, respectively.

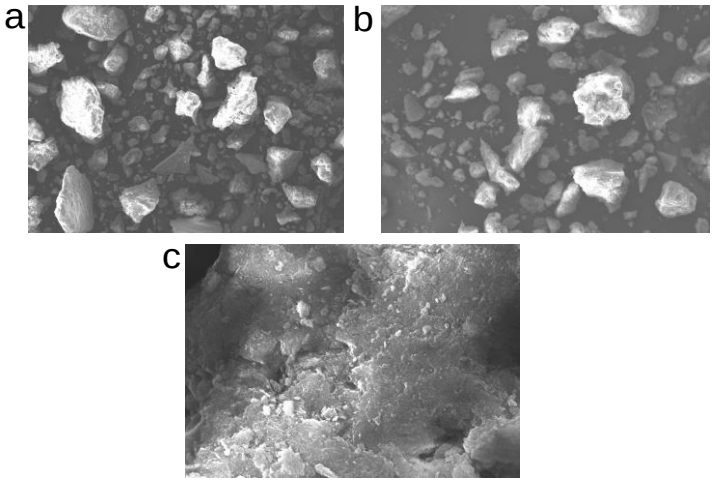

Figure 5. SEM images of **(a)** Al_2O_3; **(b)** ZnO; (**c)** Al_2O_3-Z.

3.6. Electrochemical characterization.

3.6.1. Preparation of modified glassy carbon electrode.

0.5 mg of Al_2O_3-ZnO was sonicated in IPA (isopropanol) for 30 min, and 5 µL of the resulting dispersion was drop-coated onto a previously cleaned and dried GCE at room temperature under ambient conditions.

3.6.2. Behavior of modified charge transfer electrodes.

The charge transfer behavior of the modified electrode was studied using 1mM K_4[Fe $(CN)_6$] redox probe in.0.1 M KCl solution containing 0.5 mM $K_4[Fe(CN)_6]$, shown in Figure 6a to get an insight into the electro-active behavior of the electrode. The bare GCE showed the lowest redox current intensity. When [Al_2O_3-ZnO] was immobilized on the electrode surface, the redox current intensity got enhanced as compared to the bare electrode. It indicates good conductivity due to an electron transfer resistance. The study revealed that [Al_2O_3-ZnO]/GC modified electrode is a promising electrode for electrochemical studies. The Al_2O_3-supported

ZnO electrode shows an increase in the peak current of the ferrocyanide system, indicating that [Al_2O_3-ZnO]/GC promotes faster electron transfer and provides a facile pathway for interaction between the electrode and the electrolyte. The stability and reproducible behavior of the modified electrode were assessed under good environmental conditions. The modified electrodes remained stable for 1 week, then showed a slight shift of 10 mV in the characteristic redox peak, accompanied by a decrease in peak current. This was probably due to the impairment of the orientation and stacking of the [Al_2O_3-ZnO]/GC films due to the effects of oxygen and moisture. This modified surface appeared to be more stable than previously reported SAM-modified surfaces.

3.6.3. Electrocatalytic properties of the different electrodes.

CVs from bare GCE (a), and Al_2O_3-ZnO/ GCE (b), and Al_2O_3-ZnO/ GCE with the presence of 10 µM 4-NP (c) at 50 mVs^{-1}. No redox peak current was observed at bare GCE; the peak current was observed at modified Al_2O_3-ZnO/GCE. From this, it can be concluded that the composite nanomaterial is electroactive in the selected potential range. In the absence of 4-NP, the modified GCE shows non-irreversible behavior (Figure 6 b) with relatively weak redox current peaks at Epa (anodic peak potential) = 0.549 V and Epc (cathodic peak potential) = 0.296V. However, as can be seen from Figure 7b (c), in the presence of 4-NP, a pair of well-defined redox waves on the Al_2O_3–ZnO/GCE with Epa = 0.1562 V and Epc = 0.0293 V, and the reduction potential of 4-NP becomes lower than that on the bare GCE with a positive shift of 54 mV. As expected, the redox peak currents are markedly higher (1.37×10^{-6} A) than those at the bare GCE (0.899×10^{-6} A), which suggests that Al_2O_3–ZnO is an effective mediator in the electrocatalytic redox of 4-NP, and especially the reduction peak current increased more significantly compared with the oxidation peak current. The obvious enhancement of the reduction peak current and positive shift of the reduction peak potential indicate that Al_2O_3–ZnO exhibits effective catalytic ability to reduce 4-NP, and this is due to the attractive characteristics of Al_2O_3–ZnO, such as excellent electronic properties and strong adsorptive capability. This effect demonstrates that the Al_2O_3-ZnO/GC-modified electrode exhibits strong electrocatalytic activity toward the oxidation of 4-NP.

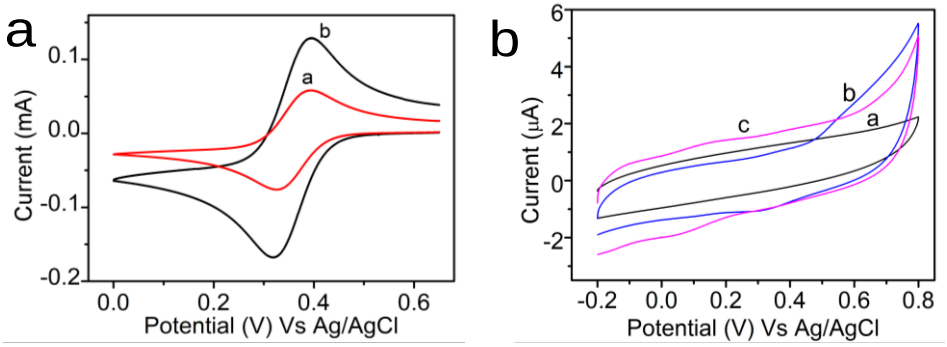

Figure 6. Charge transfer behavior of **(a)** Bare GC electrode (a), Al_2O_3-ZnO modified electrode (b); **(b)**Cyclic voltammogram of bare GC electrode (a), modified [Al_2O_3-ZnO]/GCE (b), and modified [Al_2O_3-ZnO]/GCE with 4-NP (c) in PH-7 buffer solution.

3.6.4. Electrocatalytic behavior of the Al_2O_3-ZnO/GC electrode toward 4-NP.

Cyclic voltammograms of 4-NP at bare GCE (a) and Al_2O_3-ZnO/GC electrode in buffer solution of pH 7.0 are shown in Figure 7b. At the bare GCE, 4-NP exhibited a poor electrochemical response. At the modified electrode, the voltammograms showed a redox peak

with anodic and cathodic peak potentials (Epa and Epc) of 0.1562V and 0.0293V, respectively, due to electrostatic interactions between the positively charged modifier and 4-NP. Under identical conditions, the Al2O3-ZnO/GC electrode showed a significantly higher peak current and provided clear evidence of catalytic activity. Figure 7a shows the voltammograms of 4-NP concentration variation at the Al_2O_3-ZnO/GC electrode in a buffer solution of pH 7.0, which revealed that the increase in both the anodic peak current and cathodic peak current is linear with increasing the concentration of 4-NP and a small shift in peak potential towards the negative side [34]. A linear relationship was observed between the anodic peak current and the variation in 4-NP concentration, with a correlation coefficient of 0.9961. And further, the modified electrode shows very good analytical profiles with a long linear range, sensitivity, and Lower limit of detection (LOD) are 10 to 70 µM/L, 0.0153µAµM^{-1}cm^{-2} and 3.666 µM/L, R^2 is 0.9951, and the results are reported in Table 2

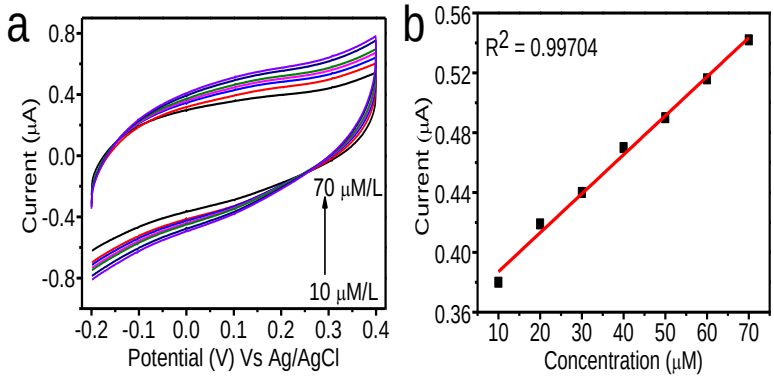

Figure 7. (a) Plot of different concentrations of 4-NP (10-70 µmol L^{-1}) at 0.15 V; **(b)** Inset graph of the peacurrent v/s various concentrations of 4-NP at a scan rate of 50 mV s^{-1} in PBS.

3.6.5.Effect of scan rate on the modified electrode.

Useful information about electrochemical mechanisms can often be obtained from the relationship between peak current and scan rate. The effect of scan rate on the redox of 4-NP was also examined.

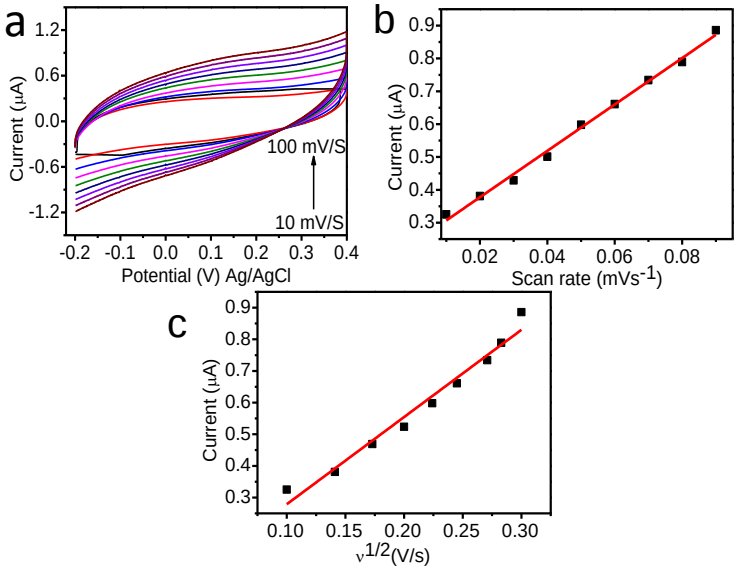

Figure 8. (a) Cyclic voltammogram of 4-NP at Al_2O_3-ZnO/GCE scanning rate ranging from (10 mV^{-1} to 100 mVs^{-1}); **(b)** Inset: Calibration graph of peak current vs scan rate; **(c)** The plot of current (I) vs. $\upsilon^{1/2}$/$mV^{1/2}s^{-1/2}$.

Figure 8 shows 70 µM 4-NP CV with Al_2O_3-ZnO/GCE with different scan rates (10-100 mVs^{-1}). With the increase in the scan rate, the reduced current gradually increased. As shown in the insert of Figure 8, the reduction current gradually increased linearly with the scan rate in the range of 10–100 mVs^{-1}, and it can be expressed as: Ipc (10^{-4} A) = 7.062 v (mVs^{-1}) + 0.236 (R^2 = 0.9944), which indicates the reduction of 4-NP on Al_2O_3-ZnO/GCE. As a result, it can be used to prevent 4-NP micro-consistency on the surface of Al_2O_3-ZnO/GCE for quantitative analysis.

Table 2. Comparison of the results for the 4-NP with the literature reports.

	Linear range (µM/L)	Technique	LOD (µM/L)	Sensitivity	Reference
rGO-Zn(II)TPEBiPc	0.02-1.0	CV	0.006	2.8784	[35]
poly(l-arginine)/CPE	50-100	CV	0.5	-	[36]
Co(II)HTC/GCE	0.2 - 10	CV	0.066	1.069	[37]
CoTBPCAPc/MWCNTs/GCE	50 to 750	CV	17 nmol L^{-1}	-	[38]
[Al_2O_3-ZnO/GCE]	10-70	CV	3.333	0.02287	**This work**

3.6.6. Reproducibility, stability, and interference.

Fabrication reproducibility for 10 modified electrodes was assessed by comparing the reduction peak current of 0.1 mM 4-NP. 3.25%, relative standard deviation(RSD) revealing that this method had excellent reproducibility.The stability of the composite GCE was also examined by measuring the composite-modified GCE response with 0.1 mM 4-NP every 10 days. Between measurements, the modified GCE was stored at 4°C in a refrigerator. The current response decreased to 90 % after 10 days, while 86 % of the original response was retained after 20 days. The GCE still retained 83% of its original response even after 30 days.

On the other hand, in order to evaluate the selectivity of the prepared sensor, the influence of some possible interfering compounds was examined in a pH7 solution (buffer) containing 4-NPat 0.1mMand0.1M, respectively (shown in Table 3). It can be seen that most phenols had no effect on the 4-NP signal, with deviations below 5%, but the nitrophenols affected the determination because they contain the same nitro groups that can be reduced near the potential of 4-NP. However, their influence is not significant at low concentrations. Additionally, some inorganic ions, such as a 500-fold concentration of Na^+, K^+, Mg^{2+}, Ca^{2+}, Ni^{2+}, Co^{2+}, Cu^{2+}, Cl^-, Br^-, I^-, NO_3^-, and SO_4^{2-}, do not influence the signals of 4-NP, with deviations below 3%. The results obtained from reproducibility, stability, and interference tests indicated that Al_2O_3–ZnO/GCE might be suitable for analytical applications. The results are discussed in Table 3.

Table 3. Influence of interferences on the determination of 4-NP (n = 3).

Interfering substances	aConcentration (µM)	Relative error (%)	Concentration (µM)	Relative error (%)
Phenol	10	0.36	01	0.12
Pyrocatechol	10	-2.12	01	1.34
Hydroquinone	10	3.53	01	-2.33
Hydroxyphenol	10	3.12	01	-1.15
Phloroglucinol	10	-1.35	01	1.26
2-Aminophenol	10	0.63	01	0.45
4-Aminophenol	10	-1.06	01	-0.69
2-Chloropheno	10	1.53	01	1.59
4-Chlorophenol	10	1.24	01	-1.62
2-Nitrophenol	10	15.32	0.1	5.35
3-Nitrophenol	10	12.71	0.1	5.27
2,4-Dinitrophenol	10	10.89	0.1	4.88

[a]Average of 10 determinations ± standard deviation

3.6.7. Analytical application.

The possibility of applying the present electrocatalysis method for 4-NP sensing in a number of real H_2O samples from the locality was evaluated. No signals for 4-NP were observed in these water samples, which may be due to the absence of 4-NP or to its concentration being below the detection limit. Thus, the 4-NP concentration was determined by the standard addition method. The results are listed in Table 3. It can be seen that the results of the proposed method for H_2O samples are in agreement with the values obtained by the HPLC method [39]. However, the HPLC method incurs higher reagent costs; in contrast, the electrochemical method offers many advantages, such as low cost, easy fabrication, and simple operation, making it worth developing. It is also clear that the recoveries obtained with the developed method are in the range of 99.0% to 102.3%. These results indicate that the proposed method is reliable, effective, and suitable for the determination of 4-NP. Additionally, the interferences in water samples can be almost neglected (see Table 4).

Table 4. Determination of 4-NP in water samples by Al_2O_3-ZnO/GCE.

Samples	Added[a] (M)	Found (M)		Relative error (%)	RSD[b] (%)	Recovery (%)
		HPLC method	Proposed method			
Drinking water	5.0	4.83	4.95	2.48	3.25	99.0
Lake water	10	9.77	9.92	1.54	3.14	99.2
River water	15	15.29	15.34	0.33	2.66	102.3
Underground H_2O	20	20.26	20.04	-1.09	4.12	100.2
Domestic sewage	25	25.45	25.28	-0.67	3.87	101.1

[a] Average value of five measurements; b Relative standard deviation for the proposed method (n = 5).

4. Conclusion

In the study, Al_2O_3-ZnO/GCE nanocatalysts were successfully synthesized by combustion and systematically characterized using spectral and structural techniques, including XRD, FTIR, UV-Vis, and SEM. The results confirm the successful incorporation of Al_2O_3 into the ZnO lattice, leading to notable changes in crystallite size and surface morphology. The enhanced surface area and improved electronic structure of the doped nanocatalyst contributed significantly to its electrochemical studies, particularly cyclic voltammetry, which demonstrated that the Al_2O_3-ZnO nanocatalyst exhibited excellent sensitivity, stability, and catalytic efficiency in the reduction of 4-nitrophenol. An electrocatalytic composite electrode for 4-NP was effectively fabricated, and the performance of this electrode was dramatically increased due to excellent electrical conductivity, strong adsorptive ability, and an excellent effective surface area of the composite-modified GCE. Thus, the modifie/GCE doped nanocatalysts present a promising, low-cost, and efficient material for environmental monitoring and remediation of nitroaromatic pollutants. Future work may explore further doping, surface modification, and real-sample analysis to expand its applicability as a practical electrochemical sensing platform.

Author Contributions

Conceptualization, S.H.K. and S.S.A.; methodology, S.H.P.; software, M.P.; validation, S.H.P., S.H.K., and S.S.A.; formal analysis, M.P.; investigation, M.P.; resources, S.S.A.;

writing—original draft preparation, M.P.; writing—review and editing, S.H.K. and S.S.A.; supervision, S.S.A. All authors have read and agreed to the published version of the manuscript.

Institutional Review Board Statement

Not applicable.

Informed Consent Statement

Not applicable.

Data Availability Statement

Data supporting the findings of this study are available upon reasonable request from the corresponding author.

Funding

This research received no external funding.

Acknowledgements

The author, Shwetha H.K., is thankful to Sahyadri Science College, Shivamogga, and JNNCE (VTU), Shimoga, Karnataka, India 577204, for providing electrochemical workstations and spectral facilities.

Conflict of interest

The authors declare no conflict of interest in this reported work.

References

1. Mulchandani, P.; Hangarter, C.M.; Lei, Y.; Chen, W.; Mulchandani, A. Amperometric microbial biosensor for p-nitrophenol using *Moraxella* sp.-modified carbon paste electrode. *Biosensors and Bioelectronics* **2005**, *21*, 523-527, https://doi.org/10.1016/j.bios.2004.11.011.
2. Niaz, A.; Fischer, J.; Barek, J.; Yosypchuk, B.; Sirajuddin; Bhanger, M.I. Voltammetric Determination of 4-Nitrophenol Using a Novel Type of Silver Amalgam Paste Electrode. *Electroanalysis* **2009**, *21*, 1786-1791, https://doi.org/10.1002/elan.200904622.
3. Lypczynska-Kochany, E. Degradation of aqueous nitrophenols and nitrobenzene by means of the Fenton reaction. *Chemosphere* **1991**, *22*, 529–536, https://doi.org/10.1016/0045-6535(91)90064-K.
4. Guo, X.; Wang, Z.; Zhou, S. The separation and determination of nitrophenol isomers by high-performance capillary zone electrophoresis. *Talanta* **2004**, *64*, 135-139, https://doi.org/10.1016/j.talanta.2004.01.020.
5. Yin, H.; Zhou, Y.; Ai, S.; Liu, X.; Zhu, L.; Lu, L. Electrochemical oxidative determination of 4-nitrophenol based on a glassy carbon electrode modified with a hydroxyapatite nanopowder. *Microchim. Acta* **2010**, *169*, 87-92, https://doi.org/10.1007/s00604-010-0309-1.
6. Castillo, M.; Domingues, R.; Alpendurada, M.F.; Barceló, D. Persistence of selected pesticides and their phenolic transformation products in natural waters using off-line liquid solid extraction followed by liquid chromatographic techniques. *Anal. Chim. Acta* **1997**, *353*, 133-142, https://doi.org/10.1016/S0003-2670(97)00353-X.
7. Niazi, A.; Yazdanipour, A. Spectrophotometric simultaneous determination of nitrophenol isomers by orthogonal signal correction and partial least squares. *J. Hazard. Mater*. **2007**, *146*, 421–427, https://doi.org/10.1016/j.jhazmat.2007.03.063.

8. Zhang, W.; Wilson, C.R.; Danielson, N.D. Indirect fluorescent determination of selected nitro-aromatic and pharmaceutical compounds via UV-photolysis of 2-phenylbenzimidazole-5-sulfonate. *Talanta* **2008**, *74*, 1400–1407, https://doi.org/10.1016/j.talanta.2007.09.016.
9. Padilla-Sánchez, J.A.; Plaza-Bolaños, P.; Romero-González, R.; Garrido-Frenich, A.; Martínez Vidal, J.L. Application of a quick, easy, cheap, effective, rugged and safe-based method for the simultaneous extraction of chlorophenols, alkylphenols, nitrophenols and cresols in agricultural soils, analyzed by using gas chromatography–triple quadrupole-mass spectrometry/mass spectrometry. *J. Chromatogr. A* **2010**, *1217*, 5724-5731, https://doi.org/10.1016/j.chroma.2010.07.004.
10. Hofmann, D.; Hartmann, F.; Herrmann, H. Analysis of nitrophenols in cloud water with a miniaturized light-phase rotary perforator and HPLC-MS. *Anal. Bioanal. Chem.* **2008**, *391*, 161-169, https://doi.org/10.1007/s00216-008-1939-6.
11. Lund, H.; Hammerich, O. Organic Electrochemistry, 4th Edition; Marcel Dekker: New York, **2001**.
12. El Mhammedi, M.A.; Achak, M.; Bakasse, M.; Chtaini, A. Electrochemical determination of *para*-nitrophenol at apatite-modified carbon paste electrode: Application in river water samples. *J. Hazard. Mater.* **2009**, *163*, 323-328, https://doi.org/10.1016/j.jhazmat.2008.06.126.
13. Yang, C. Electrochemical Determination of 4-Nitrophenol Using a Single-Wall Carbon Nanotube Film-Coated Glassy Carbon Electrode. *Microchim. Acta*. **2004**, *148*, 87–92, https://doi.org/10.1007/s00604-004-0240-4.
14. Huang, W.; Yang, C.; Zhang, S. Simultaneous determination of 2-nitrophenol and 4-nitrophenol based on the multi-wall carbon nanotubes Nafion-modified electrode. *Anal. Bioanal. Chem.* **2003**, *375*, 703-707, https://doi.org/10.1007/s00216-002-1745-5.
15. kumar, M.S.S.; Harini, H.V.; Nagaraju, G.; Nirmala, B. Combustion synthesis CuO nanoparticles: Application to photocatalytic activity. *Mater. Today Proc.* **2022**, *49*, 860-864, https://doi.org/10.1016/j.matpr.2021.06.043.
16. Sunil Kumar, S.K.; Shubha, J.P.; G, N.; N.D, R.; B, N. Facile combustion derived synthesis of copper oxide nanoparticles: Application towards photocatalytic, electrochemical and DNA cleavage studies. *Nano-Struct. Nano-Objects* **2022**, *32*, 100923,https://doi.org/10.1016/j.nanoso.2022.100923.
17. Wahab, R.; Alam, M. Highly efficient and fast electrochemical sensor based on aluminium oxide (Al_2O_3) nanoparticle for the detection of organosulfur compounds. *Sens. Actuators, A* **2022**, *347*, 113967, https://doi.org/10.1016/j.sna.2022.113967.
18. Appu, S.; Anusha, B.R.; Thilak, S.Y.; Udayabhanu; Prashantha, K. "Electrochemical sensing of Amlodipine besylate using $ZnIn_2S_4$/ZnO composite Electrodes: A High-Performance Approach". *Microchem. J.* **2025**, *214*, 113925, https://doi.org/10.1016/j.microc.2025.113925.
19. Lakshmikantha, J.; Krishnamurthy, G.; Hanumantha Nayak, R.; Pari, M.; Ranjitha, N.; Naik, N. Synthesis, structure, thermal, magnetic, dielectric properties of Ce^{3+} doped M-type $SrFe_{12}O_{19}$ and electrochemical determination of L-cysteine. *Inorg. Chem. Commun.* **2022**, *146*, 110175,https://doi.org/10.1016/j.inoche.2022.110175.
20. You, C.; Xu, X.; Tian, B.; Kong, J.; Zhao, D.; Liu, B. Electrochemistry and biosensing of glucose oxidase based on mesoporous carbons with different spatially ordered dimensions. *Talanta* **2009**, *78*, 705-710, https://doi.org/10.1016/j.talanta.2008.12.032.
21. Tang, X.; Liu, Y.; Hou, H.; You, T. A nonenzymatic sensor for xanthine based on electrospun carbon nanofibers modified electrode. *Talanta* **2011**, *83*, 1410-1414, https://doi.org/10.1016/j.talanta.2010.11.019.
22. Geim, A.K.; Novoselov, K.S. The rise of grapheme. *Nat. Mater.* **2007**, *6*, 183–191, https://doi.org/10.1038/nmat1849.
23. Dikin, D.A.; Stankovich, S.; Zimney, E.J.; Piner, R.D.; Dommett, G.H.B.; Evmenenko, G.; Nguyen, S.T.; Ruoff, R.S. Preparation and characterization of graphene oxide paper. *Nature* **2007**, *448*, 457-460,https://doi.org/10.1038/nature06016.
24. Westervelt, R.M. Graphene Nanoelectronics. *Science* **2008**, *320*, 324–325, https://doi.org/10.1126/science.1156936.
25. Zhang, X.; Huang, Y.; Wang, Y.; Ma, Y.; Liu, Z.; Chen, Y. Synthesis and characterization of a graphene–C_{60} hybrid material. *Carbon* **2009**, *47*, 334-337, https://doi.org/10.1016/j.carbon.2008.10.018.
26. Wang, H.; Cui, L.-F.; Yang, Y.; Sanchez Casalongue, H.; Robinson, J.T.; Liang, Y.; Cui, Y.; Dai, H. Mn_3O_4−Graphene Hybrid as a High-Capacity Anode Material for Lithium Ion Batteries. *J. Am. Chem. Soc.* **2010**, *132*, 13978-13980, https://doi.org/10.1021/ja105296a.

27. Zhao, J.; Chen, G.; Zhu, L.; Li, G. Graphene quantum dots-based platform for the fabrication of electrochemical biosensors. *Electrochem. Commun.* **2011**, *13*, 31-33, https://doi.org/10.1016/j.elecom.2010.11.005.
28. Nydile, T N.; Sannappa, J.; Malathesh, P.; Electrochemistry Polyaniline Ingrained Copper Oxide (PANI/CuO) Nanocomposites for Effective Electromagnetic Interference Shielding and Their Sensitive Detection of Dopamine. *Analytical & Bioanalytical Electrochemistry* **2024**, 16(7) 628-642, https://doi.org/10.22034/ABEC.2024.714686.
29. Pradeepa, K.; Shreekanta, S.A.; Raghu, G.K.; Green combustion synthesis of NiO-MgO nanocomposite using Limonia acidissima for electrochemical sensing of ascorbic acid. Chin. J. Helth Manag. **2025**, *19(10)*, 92-94, DOI-10.564220/1674-0815
30. Rezaei, B.; Damiri, S. Using of multi-walled carbon nanotubes electrode for adsorptive stripping voltammetric determination of ultratrace levels of RDX explosive in the environmental samples. *J. Hazard. Mater.* **2010**, *183*, 138-144, https://doi.org/10.1016/j.jhazmat.2010.06.127.
31. Yin, H.; Zhou, Y.; Ma, Q.; Liu, T.; Ai, S.; Zhu, L. Electrochemical oxidation behavior of guanosine-5´-monophosphate on a glassy carbon electrode modified with a composite film of graphene and multi-walled carbon nanotubes, and its amperometric determination. *Microchim. Acta* **2011**, *172*, 343-349, https://doi.org/10.1007/s00604-010-0499-6.
32. Wang, Y.; Li, Y.; Tang, L.; Lu, J.; Li, J. Application of graphene-modified electrode for selective detection of dopamine. *Electrochem. Commun.* **2009**, *11*, 889-892, https://doi.org/10.1016/j.elecom.2009.02.013.
33. Nakada, K.; Fujita, M.; Dresselhaus, G.; Dresselhaus, M.S. Edge state in graphene ribbons: Nanometer size effect and edge shape dependence. *Phys. Rev. B.* **1996**, *54*, 17954,https://doi.org/10.1103/PhysRevB.54.17954.
34. He, H.; Klinowski, J.; Forster, M.; Lerf, A. A new structural model for graphite oxide. *Chem. Phys. Lett.* **1998**, *287*, 53-56, https://doi.org/10.1016/S0009-2614(98)00144-4.
35. Pari, M.; Reddy, K.R.V.; Fassiulla; Chandrakala, K.B. Amperometric determination of dopamine based on an interface platform comprising tetra-substituted Zn2+ phthalocyanine film layer with embedment of reduced graphene oxide. *Sensors Actuators A Phys*. **2020**, *316*, 112377, https://doi.org/10.1016/j.sna.2020.112377.
36. Chandrashekar, B.N.; Swamy, B.K.; Pandurangachar, M.; Sathisha, T.V.; Sherigara, B.S. Electropolymerisation of L-arginine at carbon paste electrode and its application to the detection of dopamine, ascorbic and uric acid. *Colloids Surf. B Biointerfaces* **2011**, *88*, 413–418.
37. Afroz, L.; Khan, M.M.; Vagdevi, H.M.; Pari, M.; Shafeeualla, R.M.; Pasha, K.M. Investigation on Co(II), Ni(II), Cu(II) and Zn(II) complexes derived from novel N′-(3-hydroxybenzoyl) thiophene-2-carbohydrazide: Structural characterization, electrochemical detection of biomolecules, molecular docking and biological evaluation. *Emergent Mater*. **2022**, *5*, 1133–1155.
38. Goh, M.S.; Pumera, M. Graphene-based electrochemical sensor for detection of 2,4,6-trinitrotoluene (TNT) in seawater: the comparison of single-, few-, and multilayer graphene nanoribbons and graphite microparticles. *Anal. Bioanal. Chem.* **2011**, *399*, 127-131, https://doi.org/10.1007/s00216-010-4338-8.
39. Zhang, Y.; Sun, X.; Zhu, L.; Shen, H.; Jia, N. Electrochemical sensing based on graphene oxide/Prussian blue hybrid film modified electrode. *Electrochim. Acta* **2011**, *56*, 1239-1245, https://doi.org/10.1016/j.electacta.2010.11.011.

Publisher's Note & Disclaimer

Supplementary materials

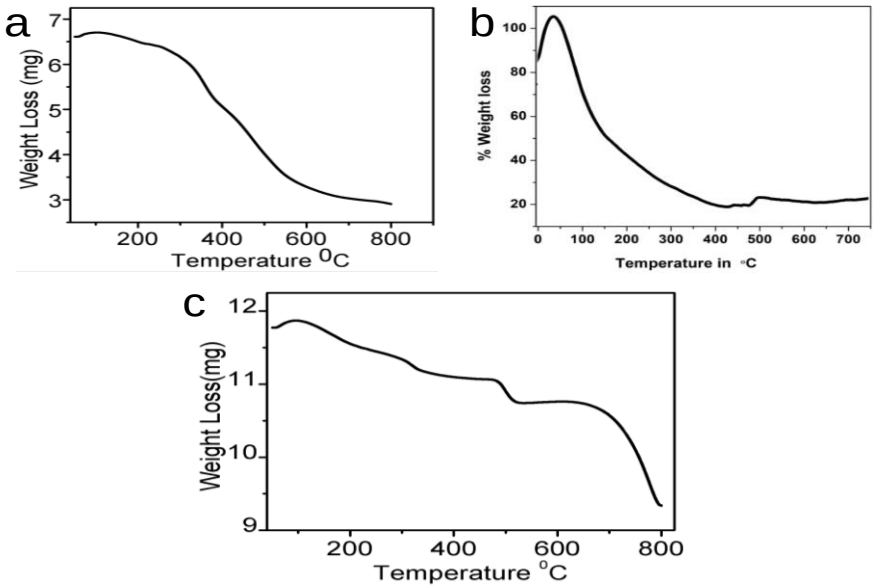

Figure S1.(a) Al_2O_3; **(b)** ZnO; **(c)** Al_2O-ZnO catalysts TGA curves of combustion method.